CHEMCOMM Communication
www.rsc.org/chemcomm

Complete characterisation of a Sb_2O_3/(21,−8)SWNT inclusion composite

Steffi Friedrichs,[a] Rüdiger R. Meyer,[b] Jeremy Sloan,*[ac] Angus I. Kirkland,[b] John L. Hutchison[c] and Malcolm L. H. Green[a]

[a] *Wolfson Catalysis Centre (Carbon Nanotechnology Group), Inorganic Chemistry Laboratory, South Parks Road, Oxford, UK OX1 3QR. E-mail: jeremy.sloan@chem.ox.ac.uk*
[b] *Department of Materials Science & Metallurgy, Pembroke Street, Cambridge, UK CB2 3QZ*
[c] *Department of Materials, Parks Road, Oxford, UK OX1 3PH*

Received (in Cambridge, UK) 13th March 2001, Accepted 12th April 2001
First published as an Advance Article on the web 2nd May 2001

The structure of a one-dimensional crystal of Sb_2O_3 encapsulated within a single-walled carbon nanotube and conformation of the latter have been solved simultaneously by high resolution transmission electron microscopy.

In this paper we report the characterisation of a one-dimensional crystal of Sb_2O_3, incorporated within a helical (21, −8) single-walled carbon nanotube (SWNT) achieved by object wave restoration from a focal series of high resolution transmission electron microscopy (HRTEM) images.† Within the nanocrystal, the atomic thickness in projection of individual antimony columns was determined and a substantial lattice contraction of the crystal along the tube axis observed. A simultaneous analysis of asymmetric fringe contrast in the tube walls provides convincing evidence for the chiral conformation of the nanotube.

SWNTs were produced using a metal catalysed arc synthesis technique similar to a method previously reported[1] and filled by capillary wetting.[2] Energy dispersive X-ray microanalysis (LINK 'ISIS' system) performed with a 0.5 nm electron probe confirmed the chemical identity of the filling material. HRTEM simulations, giving the complex wave function of the objects in question, were performed using a standard multislice algorithm[3,4] utilising a code provided by Kirkland.[5]

Fig. 1(a) shows the experimental restored HRTEM phase image of a 1.45 nm diameter SWNT containing an encapsulated single crystal of Sb_2O_3. The right tube wall displays a periodic lattice spacing of 0.224 nm, whereas the contrast variations on the left wall are effectively random. The observed periodic spacing on the right wall corresponds to the centre-to-centre spacing ($1.5d_{C–C}$ = 0.216 nm) between neighbouring 'zigzag' rows of carbon atoms in the SWNT wall lattice viewed in projection. The visibility of these spacings is determined by the SWNT conformation, the tilt angle of the cylinder relative to the electron beam and the HRTEM resolution (*ca.* 0.16 nm).

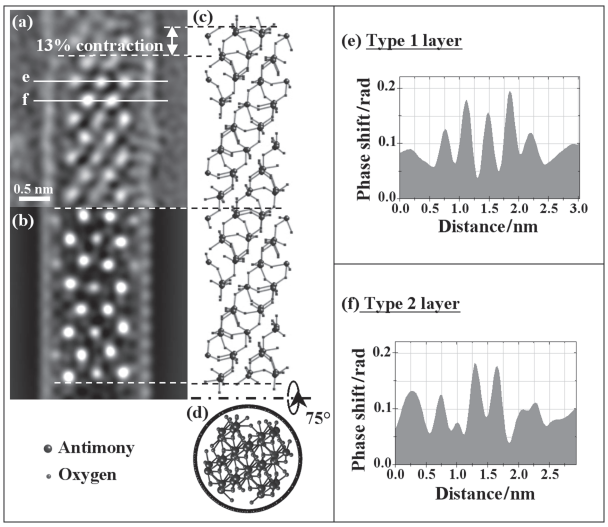

Fig. 1 Composite diagram showing the experimental restored phase image (a), the simulated phase image (b) and the structural model in the observed projection (c) and in end-on view (d), single pixel line profiles through type 1 (e) and type 2 (f) layers, respectively.

Fig. 2 illustrates the relationship between the observed wall periodicity, nanotube conformation and tilt angle together with corresponding simulations. Atomic coordinates for (*n, m*) nanotubes were generated by mapping the strip $\{\boldsymbol{r} \mid 0 \leq \boldsymbol{r} \cdot \boldsymbol{C}_h < |\boldsymbol{C}_h|^2\}$ of an unrolled hexagonal graphene lattice (with a carbon–carbon distance $d_{C–C}$ = 1.44 nm and lattice vectors $\boldsymbol{a}_1$, $\boldsymbol{a}_2$) onto a cylinder surface (Fig. 2). The structure of the SWNT is uniquely defined by the integers (*n,m*) with $n > 0$ and $-n/2 < m \leqslant n$‡ *via* the chiral vector $\boldsymbol{C}_h = n\boldsymbol{a}_1 + m\boldsymbol{a}_2$.[6] (*n*,0) and (*n*,*n*) represent the non-chiral zigzag and armchair configurations, respectively. All other (*n,m*) nanotubes are chiral with (*n* + *m*, −*m*) being the mirror image of (*n,m*).

The three differing conformation SWNTs shown in Fig. 2 (*i.e.* the (10,10) tubule in (a), the (18,0) tubule in (b) and the

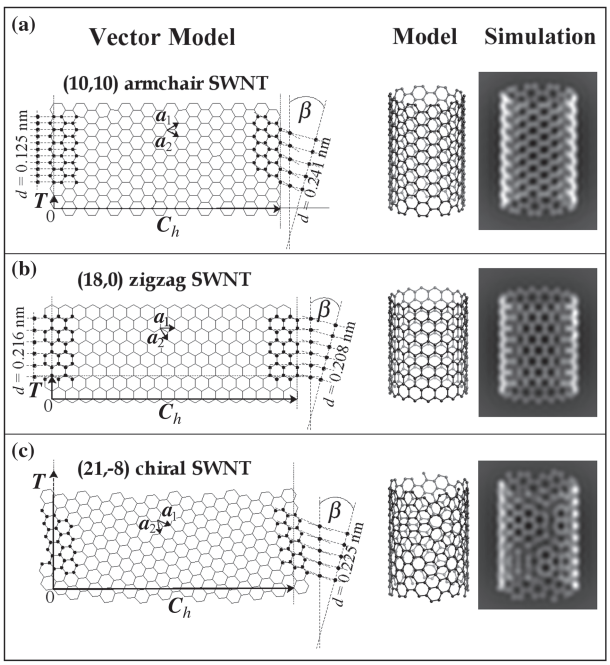

Fig. 2 (a)–(c) Schematic illustrations of the observable resolution of lattice fringes along SWNT walls of armchair, zigzag and chiral conformations, depending on the conformation, and the tilt angle β. The left column shows the unrolled graphene sheet, illustrating how the orientation of the chiral vector $\boldsymbol{C}_h$ w.r.t. the unit vectors $\boldsymbol{a}_1$ and $\boldsymbol{a}_2$ defines the rolling of a strip of the width $|\boldsymbol{C}_h|$ into a nanotube of a specific conformation and diameter. The middle column displays a modeled fraction of the SWNT, tilted by β = 15° out of the image-plane. The right column shows simulated phase images of the displayed models.

DOI: 10.1039/b102348a

(21,−8) tubule in (c)) all have diameters close to the *ca*. 1.4 nm diameter SWNT shown in Fig. 1(a).

As illustrated on the right sides of the vector models, contrast on the right tube wall is only observable when the 'zigzag' rows of carbon atoms are well aligned to the projection direction, *i.e.* when the difference $\delta_r = |\alpha - (-\beta)|$ between the chiral angle $\alpha = \angle(C_h,\boldsymbol{a}_1) = \arctan(\sqrt{3}m/(2n + m))$ and the tilt angle β of the tube axis out of the image plane is small. Similarly, contrast on the left wall is observed when $\delta_l = |\alpha - \beta|$ is small. As the numbers of atoms in projection on the tube wall is small, strong contrast will be visible for values of δ of up to 10° and the observed spacing will be given by $1.5d_{C-C}\cos\beta/\cos\alpha$ (Fig. 2(c)). For achiral tubes $\delta_l = \delta_r$ for any tilt angle and the contrast will therefore be equal on both walls. For $\beta = 0$ strong contrast will be visible on both walls of a zigzag-nanotube, whereas for the armchair tube, the difference $\delta = 30°$ is too large for an observation of any contrast due to the projection of the spacing between zigzag rows. Instead, the relevant projected spacing is that of $\sqrt{3}a/2 = 0.125$ nm between hexagon edges and centres (Fig. 1(b), left), which is too small to be resolved. For the chiral (21, −8) tube shown in Fig. 1(c), strong contrast is observed on the right wall when the top end of the tube is tilted towards the viewer. By measurement of the change in defocus along the tube, it was established that the top end of the tube was higher in the electron beam path and hence this tube must also have negative chirality.

The orientation of the incorporated crystal fraction can best be matched to an approximately $\langle 1\ 0\ -1 \rangle$ projection through a fragment of Sb_2O_3 derived from the orthorhombic valentinite structure, believed to be the high pressure form of Sb_2O_3.[7] The bulk valentinite structure consists of infinite double chains of SbO_3 units, running parallel to $\langle 0\ 0\ 1 \rangle$. In these double chains each Sb atom within the infinite Sb_2O_3 chains is coordinated by three oxygen atoms, one of which bridges between two Sb atoms.[7] The other cubic senarmonite form of antimony oxide consists of molecular Sb_4O_6 units.[8] Fig. 1(c) shows the proposed structure model (Fig. 1(d), end-on view) of the Sb_2O_3/SWNT composite.

The white spots in the reconstructed phase image represent atomic columns of antimony only in projection. The oxygen-sublattice could not be resolved, due to the weak scattering properties of oxygen and the staggering of the oxygen atoms in projection. Multislice simulations of the restored phase of Sb_2O_3 lattice fractions of appropriate thickness confirmed that the phase contrast due to the oxygen sublattice is negligible compared to that due to the antimony sublattice.

In the observed Sb_2O_3/SWNT composite the $\langle 4\ -1\ 2 \rangle$ Sb_2O_3 crystal direction, which subtends an angle of 78.3° with the optimum $\langle 1\ 0\ -1 \rangle$ viewing direction, is aligned along the tube axis. Therefore, the tube inclination of $\beta = 15°$, applied to the model and simulation in order to account for the observed contrast within the tube wall, is plausible as a small deviation from this viewing direction will not alter significantly the observed contrast of the crystal. Other preferred orientations of Sb_2O_3 were also observed but these always conformed to fragments of the valentinite strucure rather than senarmonite.

The repeating structural motif of the imaged encapsulated Sb_2O_3 crystal can be described as an alternating sequence of a layer containing three columns of Sb atoms (type 1 layer) followed by a layer containing two columns of Sb atoms (type 2 layer) arranged perpendicular to the long axis of the tube (Fig. 1(a)). Within each layer, the intensities due to the individual antimony columns vary in a complex fashion. The line profile through a type 1 layer (Fig 1(e)) shows a stacking pattern of 3–2–3 Sb atoms in projection. By contrast the line profile though a type 2 layer (Fig. 1(f)) gives two peaks of equal intensity approximately equivalent to the higher peak within the three-member layer indicating Sb columns three atoms in thickness. The multislice simulation in Fig. 1(b) also shows weak contrast close to the tube walls, resulting from single atom columns at the edge of the encapsulated crystal fragment. These were added to the periphery of the crystal model in order to account for corresponding weak peaks at these sites in the obtained phase image. However, the intensity of these peaks are not significantly higher than the background noise and it is impossible to assign these peaks to single-atom columns without a more accurate analysis of the phase contrast. The proposed model therefore consists of a Sb_2O_3 crystal fragment with sequences of 3–2–3 and (1–)3–3(–1) layers repeating every fourth equivalent layer along the $\langle 4\ -1\ 2 \rangle$ direction (Fig. 1(c)).

Since the oxygen sublattice was not resolvable, the oxygen coordination is predicted from the bulk valentinite structure. However, in order to fit the modeled Sb_2O_3 crystal into a 1.4 nm diameter SWNT, some oxygen atoms on the crystal surface were omitted. This can be justified in terms of an anticipated reduction in coordination at the Sb_2O_3/SWNT interface (*cf.* 2 × 2 and 3 × 3 KI crystals formed in SWNTs[9,10]).

Significant lattice distortions were observed in the Sb_2O_3 crystal. A comparison with the bulk structure of valentinite, shows that the encapsulated crystal displays a longitudinal contraction of 13% along the $\langle 4\ -1\ 2 \rangle$ axis (Fig. 1(a)–(c)). A similar contraction was also observed in a 3 × 3 KI crystal encapsulated within a SWNT.[9] In the Sb_2O_3/SWNT composite, lattice measurements from line traces show an average spacing of *ca*. 0.552 nm between type 1 or type 2 rows respectively, whereas in bulk Sb_2O_3 equivalent rows are spaced at *ca*. 0.638 nm. The observed lattice contraction may be caused by local interactions between the Sb_2O_3 crystal and the SWNT walls although the wall periodicity of a chiral nanotube cannot be commensurate with a periodic crystal over the long range, as was noted previously.[11] Additional distortions may be caused by the reduction in coordination at the Sb_2O_3/SWNT interface.

A more detailed account of this work is in press.[12]

We acknowledge the Petroleum Research Fund, administered by the American Chemical Society (Grant No. 33765-AC5), the EPSRC (Grant Nos. GR/L59238 and GR/L22324) and Colebrand Ltd. for financial support. S. F. is also indebted to BMBF and Fonds der Chemischen Industrie while J. S. is indebted to the Royal Society.

Notes and references

† The product was examined at 300 kV in a JEOL JEM-3000F FEGTEM (C_S = 0.57 nm; point resolution = 0.16 nm). Through focal series of individual filled nanotubes were acquired at a microscope magnification of ×600,000 using a GATAN 794 (1 k × 1 k pixel) CCD camera. From these focal series, the image wave was obtained using a Wiener filter restoration with abberations in the individual images.[11]

‡ The lower limit for *m* used here differs from the definition given in ref. 6, to ensure that the chiral angle α lies in the range $-30 < \alpha \leqslant 30°$.

1 C. Journet, W. K. Maser, P. Bernier, A. Loiseau, M. L. de la Chapelle, S. Lefrant, P. Deniard, R. Lee and J. E. Fischer, *Nature (London)*, 1997, **388**, 756.
2 J. Sloan, D. M. Wright, H.-G. Woo, S. Bailey, G. Brown, A. P. E. York, K. S. Coleman, J. L. Hutchinson and M. L. H. Green, *Chem. Commun.*, 1999, 699.
3 J. M. Cowley and A. F. Moodie, *Acta. Crystallogr.*, 1957, **10**, 609.
4 P. Goodman and A. F. Moodie, *Acta. Crystallogr., Sect. A*, 1974, **30**, 280.
5 E. J. Kirkland, in *Advanced Computing in Electron Microscopy*, Plenum Press, New York, 1998.
6 R. Saito, C. Dresselhaus and M. S. Dresselhaus, *Physical Properties of Carbon Nanotubes*, Imperial College Press, London, 1998.
7 C. Svensson, *Acta Crystallogr., Sect. B*, 1974, **30**, 458.
8 C. Svensson, *Acta Crystallogr. Sect. B*, 1975, **31**, 2016.
9 R. R. Meyer, J. Sloan, R. E. Dunin-Borowski, A. I. Kirkland, M. C. Novotny, S. R. Bailey, J. L. Hutchison and M. L. H. Green, *Science*, 2000, **289**, 1324.
10 J. Sloan, M. C. Novotny, S. R. Bailey, G. Brown, C. Xu, V. C. Williams, S. Friedrichs, E. Flahaut, R. L. Callendar, A. P. E. York, K. S. Coleman, M. L. H. Green, R. E. Dunin-Borkowski and J. L. Hutchison, *Chem. Phys. Lett.*, 2000, **329**, 61.
11 J. Sloan, J. Cook, M. L. H. Green, J. L. Hutchison and R. Tenne, *J. Mater. Chem.*, 1997, **7**, 1089.
12 S. Friedrichs, J. Sloan, J. L. Hutchinson, M. L. H. Green, R. R. Meyer and A. I. Kirkland, *Phys. Rev. B*, 2001, in press.